# Enhancement of Catalytic Activity Associated with Carbon Deposits Formed on NiO/γ-$Al_2O_3$ Catalysts during Direct Dehydrogenation of Isobutane

Shigeru SUGIYAMA[1]*, Kenta ORIBE[2], Shino ENDO[2], Tashu YOSHIDA[3], Naohiro SHIMODA[1], Masahiro KATOH[1], Yuki KATO[4], and Wataru NINOMIYA[4]

[1]*Department of Applied Chemistry, Tokushima University, Minamijosanjima, Tokushima-shi, Tokushima 770-8506, Japan*

[2]*Department of Chemical Science and Technology, Tokushima University, Minamijosanjima, Tokushima-shi, Tokushima 770-8506, Japan*

[3]*Department of Science and Technology, Tokushima University, Minamijosanjima, Tokushima-shi, Tokushima 770-8506, Japan*

[4]*Hiroshima R&D Center, Mitsubishi Chemical Corporation, 20-1, Miyuki-cho, Otake-shi, Hiroshima 739-0693, Japan*

**Keywords:** Dehydrogenation, Isobutane, Nickel oxide, Catalyst deactivation, Carbon deposition

**The dehydrogenation of isobutane in the presence of $CO_2$ over NiO supported on γ-$Al_2O_3$ was examined. For comparison, $Cr_2O_3$ supported on γ-$Al_2O_3$ was also used. It is generally accepted that a catalyst used for the dehydrogenation of various alkanes will suffer catalyst deactivation due to the formation of carbon deposits. In the present study, the yield of isobutene was significantly decreased with time-on-stream due to carbon deposition when using $Cr_2O_3$(x)/γ-$Al_2O_3$, in which x indicates the loading of a corresponding oxide by weight %. However, carbon deposits also were evident on NiO(x)/γ-$Al_2O_3$, but the yield of isobutene was enhanced with time-on-stream depending on the loading (x). This indicates that the contribution of the carbon deposition in the dehydrogenation on NiO(x)/γ-$Al_2O_3$ definitely differed from that on an ordinary catalyst system such as $Cr_2O_3$(x)/γ-$Al_2O_3$. In order to confirm the advantageous effect that carbon deposition exerted on the yield of isobutene, NiO(x)/γ-$Al_2O_3$ was first treated with isobutane and then the catalytic activity was examined. As expected, it became clear that the carbon deposits formed during the pretreatment contributed to the enhancement of the yield of isobutene. The presence of a Ni-carbide species together with the metallic Ni that was converted from NiO during dehydrogenation definitely enhanced of the yield of isobutene. Although carbon deposition is generally recognized as the main cause of catalyst deactivation, the results of the present study reveal that carbon deposition is not necessarily the cause of this phenomenon.**

## Introduction

The target material for this research was isobutene, which is an industrially important synthetic intermediate. For example, isobutene is a raw material that is used in the production of methyl methacrylate (MMA), which is a precursor monomer of poly methyl methacrylate (PMMA) and a main unit in the composition of functional chemicals such as molding materials, paints, dental materials, adhesives, textile treatment agents, leather treatment agents and resin modifiers. In Asia, $C_4$ direct oxidation, in which isobutene or isobutene-based material is used as a raw material, is employed in the production of MMA (Ninomiya *et al*., 2014). Isobutene is generally derived from ethylene via a fluid catalytic cracking (FCC) process. However, problems exist in the current method for the supply of isobutene (Nagai *et al*., 2001), and alternative supply methods are being developed. As a result, the oxidative dehydrogenation of isobutane to isobutene has been extensively examined in our laboratory. In this pursuit, the use of chromium species doped on mesoporous silicas such as MCM-41 (Ehiro *et al*., 2016), MCM-48 (Kato *et al*., 2019a), and SBM-15 (Kato *et al*., 2019b) have shown the best yields of isobutene at almost 10%. In addition, a trace amount of doping with chromium on SBA-15 has resulted in the best-known yield of isobutene at more than 16% (Kato *et al*., 2018). Without exception, however, these catalyst systems suffer from the deep oxidation to carbon oxides, which lowers the selectivity to isobutene.

In order to avoid deep oxidation, direct dehydrogenation of isobutane to isobutene was examined in the present study. Although dehydrogenation is not affected by deep oxidation, the reaction temperature is high due to the endothermic nature of the reaction, and the resultant formation of carbon deposits is followed by evident catalyst deactivation. Under such circumstances, we examined a paper on the dehydrogenation of isobutane in the presence of $CO_2$ (Ding *et al*., 2010). Although that paper reported that catalyst deactivation was evidently detected in the dehydrogenation of isobutane on NiO/γ-$Al_2O_3$ in the presence of $CO_2$, the following mechanism

Received on September 25, 2020, Accepted on XXXX, 2020

DOI:

Correspondence concerning this article should be addressed to S. Sugiyama (E-mail address: sugiyama@tokushima-u.ac.jp)

for a coupling dehydrogenation of isobutane to isobutene attracted our attention (eqs. (1) and (2)).

$$i\text{-}C_4H_{10} \rightarrow i\text{-}C_4H_8 + H_2 \quad (1)$$

$$CO_2 + H_2 \rightarrow CO + H_2O \quad (2)$$

$$C + xH_2O \rightarrow CO_x + xH_2 \quad (x = 1 \text{ or } 2) \quad (3)$$

Here, isobutane is converted to isobutene via an endothermic dehydrogenation (eq. (1)). If $CO_2$ is present in the feed stream, an endothermic reaction between $H_2$ formed from eq. (1) and $CO_2$ proceeds to form CO and $H_2O$ (reverse water gas shift reaction; eq. (2)). If $H_2O$ is formed in eq. (2), it can react with carbon (carbon deposition) via eq. (3) (endothermic stream reforming followed by exothermic water gas shift reaction), and carbon deposition, which is a serious problem in the direct dehydrogenation of isobutane, could be deleted from the surface of the catalyst.

Based on this background, the direct dehydrogenation of isobutane to isobutene in the presence of $CO_2$ was examined using $NiO/\gamma\text{-}Al_2O_3$. Since an unexpected result was obtained, a reference catalyst was also examined. $Cr_2O_3/\gamma\text{-}Al_2O_3$ was chosen as the reference catalyst, because chromium oxide is a key catalyst for the direct and oxidative dehydrogenation of isobutane to isobutene (Carrà and Forni, 1971; Grzybowska *et al*., 1998; Jibril *et al*., 2005; Korhonen *et al*., 2007).

## Experimental section

### 1.1 Preparation of catalysts

The impregnation method was used to prepare $NiO(x)/\gamma\text{-}Al_2O_3$ and $Cr_2O_3(x)/\gamma\text{-}Al_2O_3$, according to a previously reported method (Ding *et al*., 2010). The values in parentheses indicate the content by weight %. Preparation of the $NiO(20)/\gamma\text{-}Al_2O_3$ began with 20 mL of aqueous solution into which we dissolved 3.93 g of $Ni(NO_3)_2{\cdot}6H_2O$ (Wako Pure Chemical Industries, Ltd.) and 4.01 g of $\gamma\text{-}Al_2O_3$ (JRC-ALO-9, which served as reference catalysts, and were supplied from The Catalysis Society of Japan). The preparation of $Cr_2O_3(20)/\gamma\text{-}Al_2O_3$ began with 20mL of aqueous solution into which we dissolved 6.58 g of $Cr(NO_3)_3{\cdot}9H_2O$ (Sigma-Aldrich Co. LLC.) and 4.01 g of $\gamma\text{-}Al_2O_3$ (JRC-ALO-9, a reference catalyst supplied from The Catalysis Society of Japan). Each of these suspensions was then evaporated to dryness and dried at 383 K for 12 h. Finally, the resultant solid was calcined at 823 K.

### 1.2 Characterization of catalysts

X-ray diffraction (XRD) patterns were obtained using a SmartLab/R/INP/DX (Rigaku Co.) with a Cu Kα radiation monochromator at 45 kV and 150mA. Nitrogen adsorption isotherms of the catalysts pretreated at 473 K for 5 h were measured using a BELSORPmax12 (MicrotracBEL) at 77 K, and then the specific surface areas were estimated via BET. The acidic properties of the catalysts were measured for $NH_3$ temperature-programed desorption ($NH_3$-TPD) using a BELCAT (MicrotracBEL) under the following conditions. First, each catalyst was exposed to 50 sccm of He gas flow at 773 K for 1 h as a pretreatment. Second, each catalyst was treated under 50 sccm of a 5% $NH_3$/He gas flow for 30 min at 373 K to promote the adsorption of $NH_3$ as a main treatment. Finally, the catalysts were maintained under He gas at 50 sccm for 15 min and were then heated from 373 K to 883 K (heating rate = 10 K/min) under a flow of He gas at 30 sccm. The desorbed $NH_3$ from the catalyst was then monitored using a BELMass (MicrotracBEL) quadruple mass spectrometer, which showed a mass signal of m/e = 16 for $NH_3$. Given that the $NH_3$ parent peak showed a mass signal of m/e = 17, however, the desorbed $NH_3$ is thought to have been strongly influenced by $H_2O$. In order to analyze the properties of the carbon deposits that formed on the catalyst, temperature-programmed oxidation (TPO) using a BELCAT (MicrotracBEL) was employed. Each catalyst previously used in the catalytic

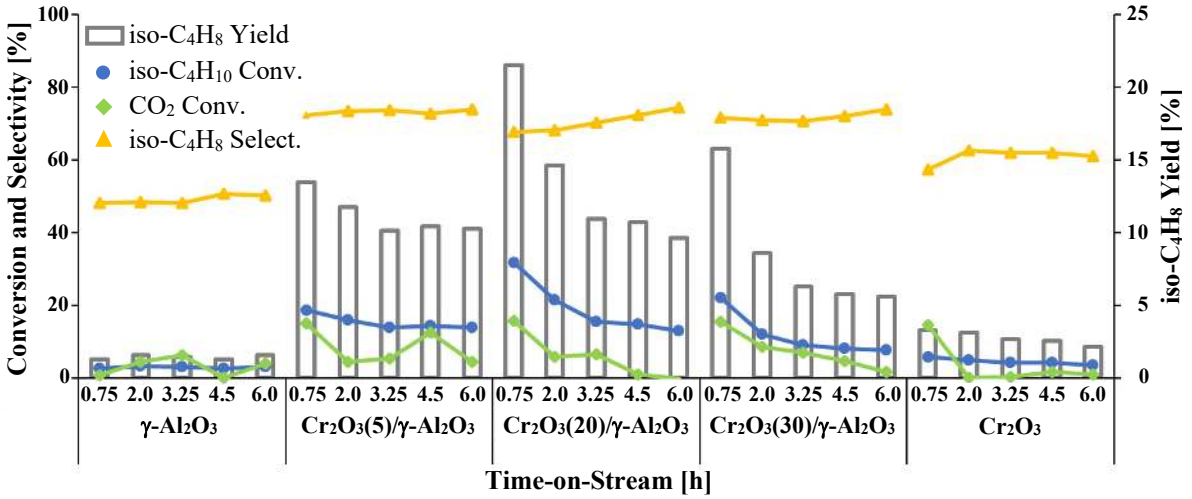


**Fig. 1** Catalytic performances when using $\gamma\text{-}Al_2O_3$, $Cr_2O_3(x)/\gamma\text{-}Al_2O_3$ (x=5, 20, 30), and $Cr_2O_3$ for the dehydrogenation of isobutane at 823 K

reaction was exposed to 50 sccm of a gas flow consisting of $O_2$ (10 sccm) and He (40 sccm) during heating to 973 K at a heating rate of 5 K/min. During the heating, the desorpted amounts of $CO_2$ were analyzed using a quadruple mass spectrometer (BELMass, MicrotracBEL), which showed mass signals of m/e = 44 for $CO_2$. Field emission scanning electron microscopy (FE-SEM) images of the samples were recorded using a JSM-7400F (JEOL Ltd.). Thermogravimetric analysis (TGA) was carried out using a ThermoPlus Evo TG8120 (Rigaku Co.).

### 1.3 Evaluation of catalytic performances

For the catalytic activity test, a fixed-bed continuous flow reactor was operated at atmospheric pressure and 823 K. Each catalyst was pelletized and sieved to reach a size of 0.85-1.70 mm and a weight of 0.25 g. The temperature of the catalyst bed was increased to 823 K under a flow of He. After the reaction temperature was stabilized, tests were carried out under 15 mL/min of a reactant gas flow that consisted of $P$(iso-$C_4H_{10}$) = 14.1 kPa, $P(CO_2)$ = 12.3 kPa, and $P$(He) = 74.9 kPa. Pretreatment with isobutene first involved the use of a pretreatment gas (isobutane) introduced at 2.1 mL/min for a pre-set time following temperature stabilization. Homogeneous reactions were negligible under these conditions. The reaction products were detected via an on-line gas chromatograph (GC-8APT, Shimadzu Corp.) that involved the use of a thermal conductivity detector (TCD) and a capillary gas chromatograph (GC-2025, Shimadzu Corp.) equipped with a flame ionization detector (FID). The columns in the TCD-GC consisted of a Molecular Sieve 5A (0.2 m×Φ3 mm) for the detection of $O_2$, $CH_4$, and CO and a HayaSep R (0.2 m×Φ 3 mm) for the detection of $CO_2$, $C_2$, $C_3$, and $C_4$ species. An Rt-Almina BOND/$Na_2SO_4$ (30 m×Φ 0.53 mm) was used as a capillary column in the FID-GC to provide detailed characterizations of the $C_4$ species. The conversion and the selectivity were estimated on a carbon basis. The yield of isobutene was calculated from the product of the conversion of isobutane and the selectivity to isobutene.

## 2. Results and Discussions

### 2.1 Catalytic performances

**Figure 1** shows the catalytic performances for the dehydrogenation of isobutane at 823 K on γ-$Al_2O_3$, $Cr_2O_3$(x)/γ-$Al_2O_3$ (x=5, 20, 30), and $Cr_2O_3$. The conversions of isobutane and the yields of isobutene for γ-$Al_2O_3$ and $Cr_2O_3$ were quite low. However, when γ-$Al_2O_3$ was doped with $Cr_2O_3$, the conversion and the yield were evidently enhanced for the resultant $Cr_2O_3$(x)/γ-$Al_2O_3$. For example, the conversion and yield were enhanced 31.8 and 21.5%, respectively, at 0.75 h on-stream on $Cr_2O_3$(20)/γ-$Al_2O_3$. Since 2013, our group has focused on developing highly active catalysts for the oxidative dehydrogenation of isobutane to isobutene (Sugiyama *et al*., 2013), which finally led to an active catalyst of SBA-15 doped with chromium that produced an isobutene yield of 16.8% (Kato *et al*., 2018). By using the present method for the direct dehydrogenation of isobutane to isobutene, however, we have already achieved a yield of isobutene that exceeds that obtained from oxidative dehydrogenation. Unfortunately, this great level of activity was evidently reduced by time-on-stream. In a direct dehydrogenation reaction, such a decrease in activity due to the passage time generally accepted as inevitable.

**Figure 2** shows the catalytic performances for the dehydrogenation of isobutane at 823 K on γ-$Al_2O_3$, NiO(x)/γ-$Al_2O_3$ (x=5, 20, 30), and NiO. The low

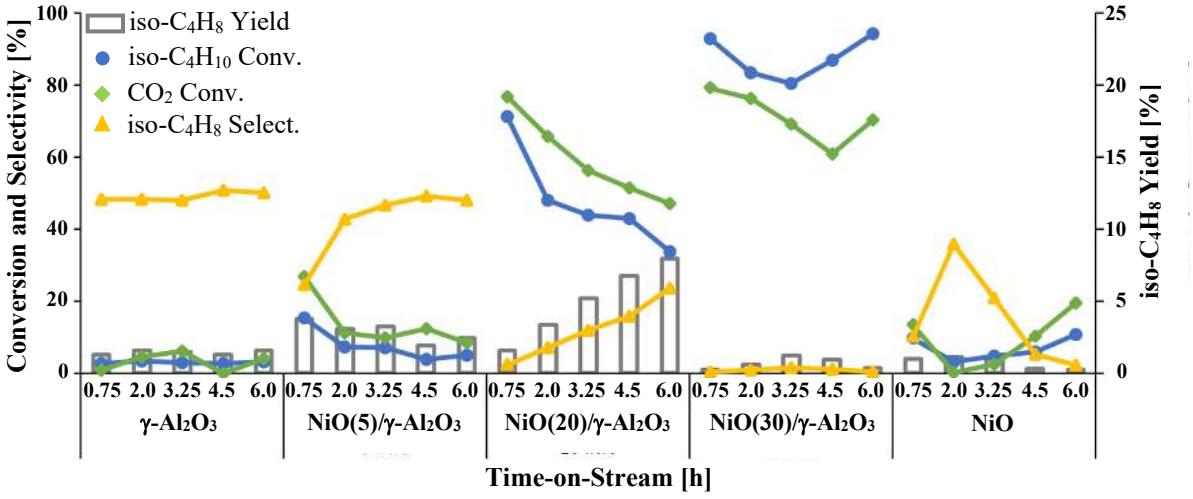


**Fig. 2** Catalytic performances when using γ-$Al_2O_3$, NiO(x)/γ-$Al_2O_3$ (x=5, 20, 30), and NiO for the dehydrogenation of isobutane at 823 K

conversion of isobutane and the yield of isobutene were again observed on NiO. In contrast to the dehydrogenation of isobutane on $Cr_2O_3(x)/\gamma\text{-}Al_2O_3$, doping with 5, 20 and 30 wt% of NiO on $\gamma\text{-}Al_2O_3$ showed improvement in neither the conversion nor the yield at 0.75 h on-stream. However, we noted an unusual behavior when using this catalyst. When $NiO(20)/\gamma\text{-}Al_2O_3$ was used, the yield of isobutene was evidently improved with increases in the time-on-stream. The yield of isobutene was 1.6% at 0.75 h on-stream, but was improved to 7.9% at 6 h on-stream. A similar enhancement in the yield of isobutene was also detected on $NiO(18)/\gamma\text{-}Al_2O_3$ from 1.8% at 0.75 h to 9.5% at 6 h on-stream; and, on $NiO(23)/\gamma\text{-}Al_2O_3$ from 0.2% at 0.75 h to 3.5% at 6 h on-stream. Therefore, the enhancement of the yield of isobutene on $NiO(20)/\gamma\text{-}Al_2O_3$ was not observed with a special loading of nickel species, but it was confirmed that enhancement was commonly observed after a loading with a certain width on $\gamma\text{-}Al_2O_3$. The deactivation results as observed in the yield of isobutene on $Cr_2O_3(x)/\gamma\text{-}Al_2O_3$ were generally accepted in the direct dehydrogenation of alkane. As far as we could ascertain, however, there has been no report of the yield enhancement found in the present study by using $NiO(x)/\gamma\text{-}Al_2O_3$ (x = 18, 20 and 23). Therefore, characterizations using fresh samples of $Cr_2O_3(x)/\gamma\text{-}Al_2O_3$ and $NiO(x)/\gamma\text{-}Al_2O_3$ were carried out.

### 2.2 Characterization of fresh catalysts

XRD, nitrogen adsorption isotherm measurements and $NH_3$-TPD were carried out for analysis of the structural and acidic properties of fresh catalysts. The XRD patterns of fresh $Cr_2O_3(x)/\gamma\text{-}Al_2O_3$ and $NiO(x)/\gamma\text{-}Al_2O_3$ together with $Cr_2O_3$, NiO, and $\gamma\text{-}Al_2O_3$ are shown in **Figures 3 (A)** and **(B)**, respectively.

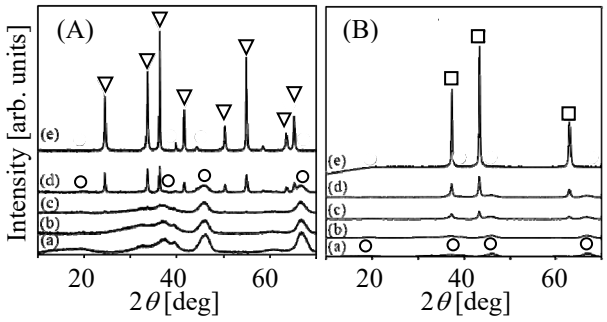


**Fig. 3** XRD patterns of fresh (A) $Cr_2O_3(x)/\gamma\text{-}Al_2O_3$ and (B) $NiO(x)/\gamma\text{-}Al_2O_3$. (a) $\gamma\text{-}Al_2O_3$, (b), (c) and (d) for x= 5, 20 and 30, respectively, and (e) $Cr_2O_3$ (A) or NiO (B).
○: $\gamma\text{-}Al_2O_3$, ▽: $Cr_2O_3$, □: NiO

As expected, XRD peaks due to $Cr_2O_3$ (JCPDS 00-059-0308) and $\gamma\text{-}Al_2O_3$ (JCPDS 00-010-0425) were detected from $Cr_2O_3(x)/\gamma\text{-}Al_2O_3$ while peaks for NiO (JCPDS 03-065-6920) and $\gamma\text{-}Al_2O_3$ were detected from $NiO(x)/\gamma\text{-}Al_2O_3$. Therefore, no formations of complex oxide that consisted of the support and each oxide were detected.

**Table 1** shows the specific surface areas and acid amounts for fresh $Cr_2O_3(x)/\gamma\text{-}Al_2O_3$ and $NiO(x)/\gamma\text{-}Al_2O_3$ together with $Cr_2O_3$, NiO, and $\gamma\text{-}Al_2O_3$. Specific surface areas and acid amounts on $Cr_2O_3(x)/\gamma\text{-}Al_2O_3$ and $NiO(x)/\gamma\text{-}Al_2O_3$ were decreased with increases in each loading.

**Table 1** Specific surface area and acid amount for fresh $Cr_2O_3(x)/\gamma\text{-}Al_2O_3$ and $NiO(x)/\gamma\text{-}Al_2O_3$ together with catalytic active species and the support

| Catalyst | Surface area [$m^2/g$] | Acid amount [mmol/g] |
|---|---|---|
| $\gamma\text{-}Al_2O_3$ | 210 | 0.304 |
| $Cr_2O_3(5)/\gamma\text{-}Al_2O_3$ | 199 | 0.222 |
| $Cr_2O_3(20)/\gamma\text{-}Al_2O_3$ | 188 | 0.222 |
| $Cr_2O_3(30)/\gamma\text{-}Al_2O_3$ | 160 | 0.091 |
| $Cr_2O_3$ | 9 | 0.029 |
| $NiO(5)/\gamma\text{-}Al_2O_3$ | 199 | 0.399 |
| $NiO(20)/\gamma\text{-}Al_2O_3$ | 156 | 0.291 |
| $NiO(30)/\gamma\text{-}Al_2O_3$ | 142 | 0.218 |
| NiO | 13 | 0.046 |

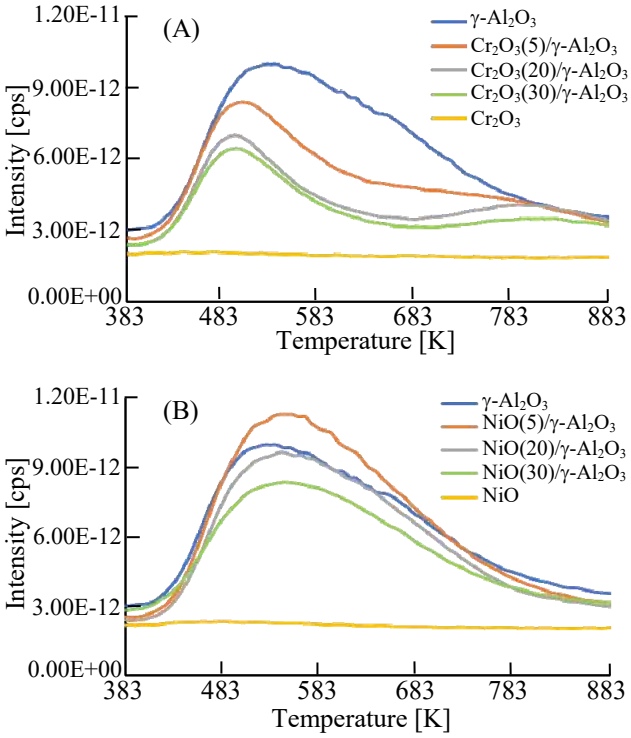


**Fig. 4** $NH_3$-TPD of fresh (A) $Cr_2O_3(x)/\gamma\text{-}Al_2O_3$ and (B) $NiO(x)/\gamma\text{-}Al_2O_3$ together with catalytic active species and the support.

Since the only special effect on these properties was the magnitude of the relationship, ammonia TPD

was examined. **Figures 4 (A)** and **(B)** list the $NH_3$-TPD results for $Cr_2O_3(x)/\gamma\text{-}Al_2O_3$ and $NiO(x)/\gamma\text{-}Al_2O_3$ (x=5, 20 and 30). As a reference, the $NH_3$-TPD results for $\gamma\text{-}Al_2O_3$ and each single oxide were added. Comparing $Cr_2O_3(x)/\gamma\text{-}Al_2O_3$ and $NiO(x)/\gamma\text{-}Al_2O_3$ showed an evident decrease in the stronger acidic sites for $Cr_2O_3(x)/\gamma\text{-}Al_2O_3$ with increases in loading (x). Therefore, we confirmed that stronger acidic sites remained in $NiO(x)/\gamma\text{-}Al_2O_3$, the use of which significantly improved the yield of isobutene with time-on-stream. It is evident that the results shown in Table 1 and Figure 4 are correlated to the activity on $Cr_2O_3(x)/\gamma\text{-}Al_2O_3$ (Figure 1) but are not correlated to that on $NiO(x)/\gamma\text{-}Al_2O_3$ (Figure 2). Therefore, this indicates that $NiO(x)/\gamma\text{-}Al_2O_3$ possesses completely different activity-expressing factors from those of $Cr_2O_3(x)/\gamma\text{-}Al_2O_3$.

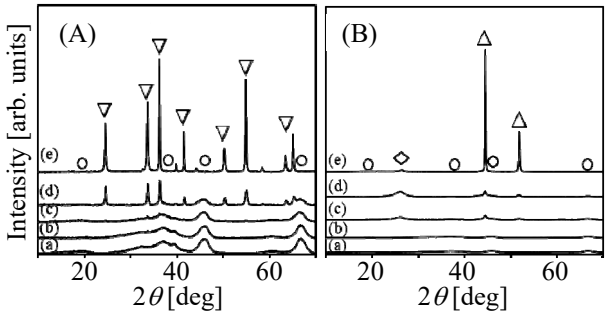


**Fig. 5** XRD patterns of (A) $Cr_2O_3(x)/\gamma\text{-}Al_2O_3$ and (B) $NiO(x)/\gamma\text{-}Al_2O_3$. (a) $\gamma\text{-}Al_2O_3$, (b), (c) and (d) for x= 5, 20 and 30, respectively, and (e) $Cr_2O_3$ (A) or NiO (B) previously used for obtaining the results shown in Figs. 1 and 2. ○: $\gamma\text{-}Al_2O_3$, ▽: $Cr_2O_3$, △: Ni, ◇: Carbon

The XRD for $Cr_2O_3(x)/\gamma\text{-}Al_2O_3$ and $NiO(x)/\gamma\text{-}Al_2O_3$ previously used to obtain the results shown in Figures 1 and 2 (**Figures 5 (A)** and **(B)**, respectively) further provided noticeable results. As shown in Figure 5 (A), the XRD patterns of $Cr_2O_3(x)/\gamma\text{-}Al_2O_3$ before and after dehydrogenation (Figure 3 (A) and Figure 5 (A), respectively) were essentially identical. In contrast, $NiO(x)/\gamma\text{-}Al_2O_3$ before and after the reaction (Figure 3 (B) and Figure 5 (B), respectively) demonstrated the effects of carbon deposition (JCPDS 01-071-4630) and the reduction of NiO to Ni (JCPDS 00-004-0850) after the reaction. Therefore, the formation of carbon deposits and metallic Ni contributed to an enhancement of the yield of isobutene with time-on-stream particularly on $NiO(20)/\gamma\text{-}Al_2O_3$. The remainder of this paper focuses on $NiO(20)/\gamma\text{-}Al_2O_3$ in order to investigate the cause of the increase in the yield of isobutene with time-on-stream.

### 2.3 Catalytic activity on $NiO(20)/\gamma\text{-}Al_2O_3$

In order to examine the carbon deposition and conversion from NiO to metallic Ni during the reaction and its effect on the improvement of the yield of isobutene, as shown above, a normal catalytic activity test was performed on $NiO(20)/\gamma\text{-}Al_2O_3$ pretreated with isobutane at 2.1 mL/min for a pre-set time at 823 K. As shown in **Figure 6**, the initial yield of isobutene at 0.75 h on-stream increased from 1.6 to 1.7, 6.8, 11.7, and 12.5% with pre-set times that ranged from 0 to 1, 3, 5, and 7 h, respectively. Regardless of the pretreatment times, the yield of isobutene was increased with time-on-stream. When the pretreatment time was increased from 0 to 1, 3, 5, and 7 h, the yield of isobutene at 6 h on-stream was improved from 7.9 to 9.1, 16.4, 18.6, and 15.9%, respectively. The best yield of isobutene (18.6%) in the present study was higher than the results achieved in the oxidative dehydrogenation of isobutane to isobutene on Cr-doped SBA-15 over a period of 5 years (Sugiyama *et al*., 2013; Kato *et al*., 2018). **Table**

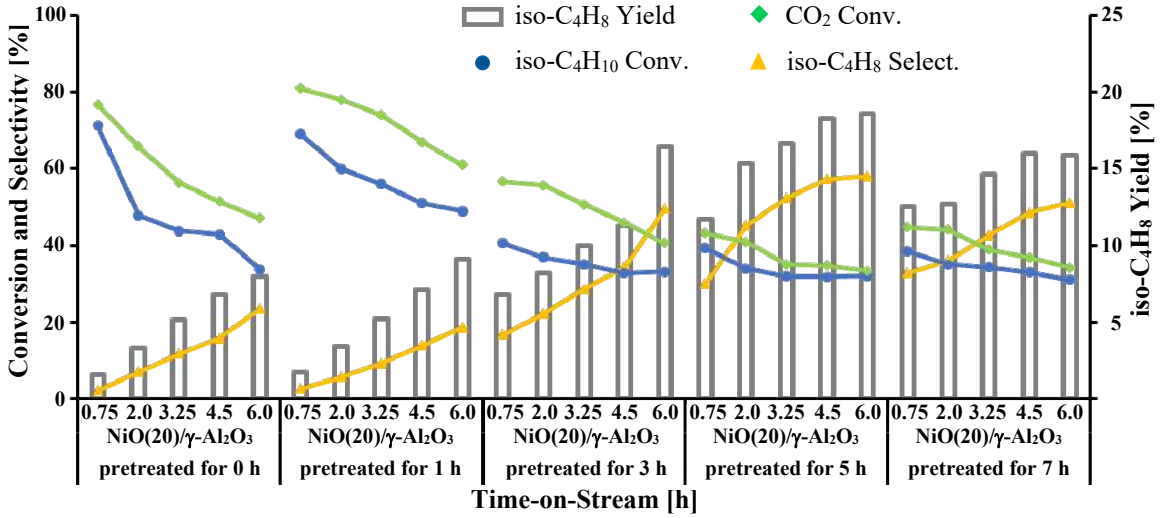


**Fig. 6** Catalytic performances for the dehydrogenation of isobutane at 823 K on $NiO(20)/\gamma\text{-}Al_2O_3$ pretreated with iso-$C_4H_{10}$ for a pre-set time at 823 K.

**2** lists the selectivities to each of the reaction by-products, which include the conversions of iso-$C_4H_{10}$ and $CO_2$ as well as the iso-$C_4H_8$ selectivity and yield, that appear in Figure 6. Although $C_2H_4$ and $C_2H_6$ were sometimes produced, selectivities to both $C_2$ species were less than 0.2%. It was evident that CO was formed via eqs. (1) and (2), while the contribution of eq. (3) seemed negligible (see below). $CH_4$ and $C_3$ species were also detected due to the catalytic nature of the Ni-catalyst, which is generally known as an active catalyst for cracking reactions. Since the selectivity to $CH_4$ was greater than those to any of the $C_3$ species, the cracking reaction of the $C_3$ species to $CH_4$ could proceed.

**Table 2** Selectivity to the by-products produced on NiO(20)/γ-$Al_2O_3$, in conjunction with the results shown in Figure 6.

| Pre-set time[a] [h] | TOS[b] [h] | Selectivity [%] $CH_4$ | CO | $C_3H_6$ | $C_3H_8$ |
|---|---|---|---|---|---|
| 0 | 0.75 | 21.4 | 74.5 | 0.2 | 1.5 |
| | 2.0 | 7.3 | 83.1 | 0.3 | 2.4 |
| | 3.25 | 4.7 | 79.5 | 0.5 | 3.5 |
| | 4.5 | 4.2 | 75.2 | 0.6 | 4.3 |
| | 6.0 | 3.6 | 66.2 | 0.9 | 5.6 |
| 1 | 0.75 | 27.2 | 70.2 | 0.1 | 0.0 |
| | 2.0 | 18.6 | 75.5 | 0.1 | 0.0 |
| | 3.25 | 14.9 | 75.5 | 0.3 | 0.0 |
| | 4.5 | 10.5 | 75.1 | 0.5 | 0.0 |
| | 6.0 | 9.1 | 71.7 | 0.6 | 0.0 |
| 3 | 0.75 | 9.8 | 73.0 | 0.5 | 0.0 |
| | 2.0 | 8.7 | 68.6 | 0.6 | 0.0 |
| | 3.25 | 7.5 | 63.1 | 0.9 | 0.0 |
| | 4.5 | 10.0 | 54.5 | 1.2 | 0.0 |
| | 6.0 | 5.0 | 44.0 | 1.5 | 0.0 |
| 5 | 0.75 | 8.5 | 60.4 | 1.0 | 0.0 |
| | 2.0 | 8.8 | 46.1 | 0.0 | 0.0 |
| | 3.25 | 7.5 | 37.7 | 2.1 | 0.0 |
| | 4.5 | 4.4 | 35.6 | 2.3 | 0.0 |
| | 6.0 | 4.2 | 35.4 | 2.3 | 0.0 |
| 7 | 0.75 | 6.7 | 59.3 | 1.4 | 0.0 |
| | 2.0 | 6.0 | 56.4 | 1.5 | 0.0 |
| | 3.25 | 5.4 | 50.2 | 1.8 | 0.0 |
| | 4.5 | 5.1 | 43.9 | 2.2 | 0.0 |
| | 6.0 | 4.7 | 41.7 | 2.2 | 0.0 |

[a]Pre-set time for pretreatment with iso-$C_4H_{10}$.
[b]Time-on-stream

In order to examine whether the high enhancement using NiO(20)/γ-$Al_2O_3$ was maintained in a steady state, the activity test on this catalyst was re-tested for 10.5 h on-stream under the same conditions shown in Figure 6 with a preset time fixed at 5 h. Although the results shown in **Figure 7** differ from those in Figure 6, the difference is slight. Isobutane conversion showed was the maximum at 0.75 h on-stream and the conversion was clearly lower than the equilibrium conversion, approximately 60%, which was estimated from data reported by Okada (2005). A high isobutene yield was maintained for 4.5 to 9 h on-stream, but the isobutene yield was clearly reduced at 10.5 h on-stream. The cause will be described in the final section of this paper.

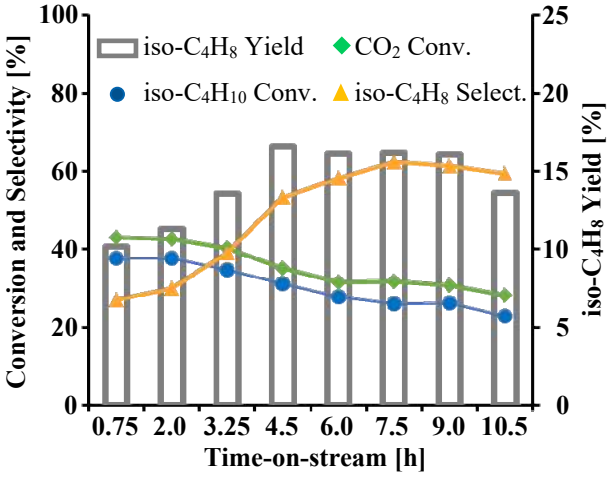


**Fig. 7** Effect that a longer time-on-stream exerted on the dehydrogenation of isobutane at 823 K on NiO(20)/γ-$Al_2O_3$ pretreated with iso-$C_4H_{10}$ for 5 h at 823 K.

When using the pretreatment gas, carbon deposition and reduction from NiO to metallic Ni is expected to proceed simultaneously. Therefore, instead of a pretreatment gas consisting of isobutane, hydrogen gas diluted with nitrogen [$P(H_2)$ = 20.2 kPa, F = 60 mL/min] was used for the pretreatment. As shown in **Figure 8**, although enhancement in the yield of isobutene was observed on NiO(20)/γ-$Al_2O_3$ treated with the hydrogen gas for pre-set times of 1 and 5 h at 823 K, the enhancement rate was rather negligible.

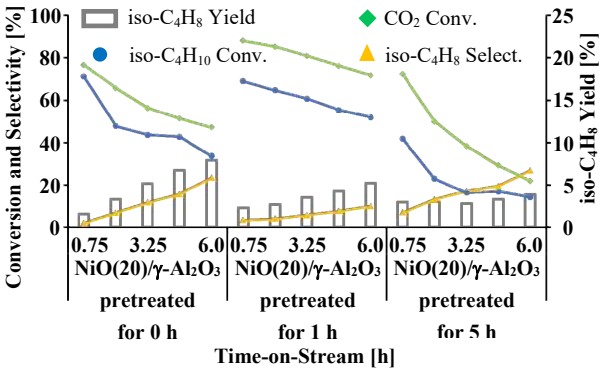


**Fig. 8** Catalytic performances for the dehydrogenation of isobutane at 823 K on NiO(20)/γ-$Al_2O_3$ pretreated with $H_2$ for 0, 1 and 5 h at 823 K.

In order to compare the crystal size of the metallic Ni formed on NiO(20)/γ-$Al_2O_3$ during the pretreatment

using iso-$C_4H_{10}$ and $H_2$, the crystal size of Ni was calculated using the XRD peak at $2\theta = 44$ degrees for (112) plane due to the metallic Ni based on the Scherrer equation, which is summarized in **Table 3**. The crystal size was smaller than 100 nm, which was outside the range of Scherrer equation (Ohtani, 2005), but was used for semi-quantitative discussion. The pretreatment and reaction conditions were the same for both Figures 6 and 8. In the case of iso-$C_4H_{10}$ pretreatment, the crystal sizes of the catalyst pretreated for 0 and 1 h were greater than 74 Å regardless of the use of the reaction. However, pretreatment for longer than 3 h resulted in a crystal size that was smaller than 39 Å regardless of the reaction conditions. By contrast, the crystal sizes of the catalyst pretreated with $H_2$ for 1 and 5 h followed by the use of the same reaction conditions were greater than 71 Å. Therefore, the pretreatment of $H_2$ certainly contributed to the increase in the sintering of metallic Ni. Although metallic Ni obtained after the iso-$C_4H_{10}$ pretreatment for longer than 3 h showed a higher rate of dispersion than that pretreated with $H_2$, the lower activity shown in Figure 8 cannot be explained only by the effect of the sintering. It should be noted that this XRD peak at $2\theta = 44$ degrees may contain information other than metallic Ni, as will be described in the final section of the present paper. Therefore, carbon deposits formed during pretreatment with isobutane seemed to improve the enhancement, as shown in Figure 6. It should be noted that the rate of improvement in the yield decreased with increases in pretreatment time. Therefore, NiO(20)/γ-$Al_2O_3$ pretreated for 0 and 5 h were carefully characterized after obtaining the results shown in Figure 6.

**Table 3** Crystal size of metallic Ni formed on NiO(20)/γ-$Al_2O_3$

| Pretreatment gas | Pretreatment time [h] | Reaction time [h] | Crystal size [Å] |
|---|---|---|---|
| iso-$C_4H_{10}$ | 1 | 0 | 74 |
| | 5.0 | 0 | 34 |
| | 0 | 6.0 | 90 |
| | 1.0 | 6.0 | 75 |
| | 3.0 | 6.0 | 30 |
| | 5.0 | 6.0 | 29 |
| | 7.0 | 6.0 | 39 |
| $H_2$ | 1.0 | 6.0 | 71 |
| | 5.0 | 6.0 | 93 |

### 2.4 Characterization of NiO(20)/γ-$Al_2O_3$ previously used for the reaction

**Figures 9 (A)** and **(B)** display photos of NiO(20)/γ-$Al_2O_3$ following pretreatment for 0 and 5 h based on the results shown in Figure 6. The formation of an excess amount of carbon deposits on NiO(20)/γ-$Al_2O_3$ pretreated for 5 h (Figure 9 (B)) was more evident than that on the catalysts pretreated for 0 h (Figure 9 (A)). Thermogravimetric analyses revealed that the carbon deposition rate of NiO(20)/γ-$Al_2O_3$ pretreated for 5 h was 78.0%, but that of NiO(20)/γ-$Al_2O_3$ pretreated for 0 h was 46.8%. It is noteworthy that the previously obtained carbon deposition rates for the inlet and outlet sides of NiO(20)/γ-$Al_2O_3$ were 89.7 and 78.6%, respectively, as shown in Figure 7. The carbon deposition rate was obtained by subtracting the weight loss due to moisture when heating to 473K from the weight loss due to carbon deposition when heating to 873K in the catalyst, followed by dividing by the weight of the catalyst before heating.

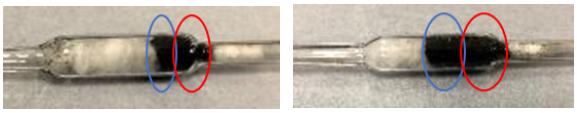

(A) (B)

**Fig. 9** Photos of NiO(20)/γ-$Al_2O_3$ pretreated for (A) 0 and (B) 5 h but after obtaining the results shown in Figure 6.
Blue circle: inlet side. Red circle: outlet side.

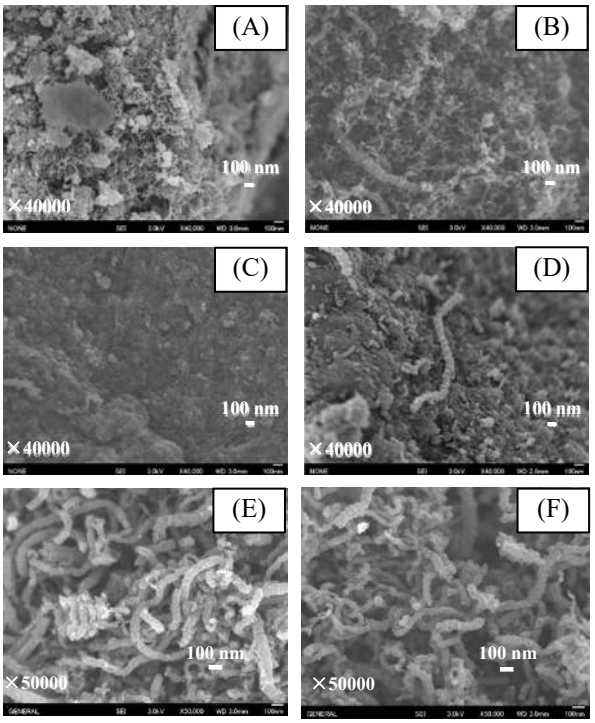


**Fig. 10** FE-SEM images ((A)-(D)) of NiO(20)/γ-$Al_2O_3$ previous used for obtaining the results shown in Figure 6 and those ((E)-(F)) in Figure 7
(A) Inlet side of the catalyst pretreated for 0 h.
(B) Outlet side of the catalyst pretreated for 0 h.
(C) Inlet side of the catalyst pretreated for 5 h.
(D) Outlet side of the catalyst pretreated for 5 h.
(E) Inlet side of the catalyst after used for 10.5 h.
(F) Outlet side of the catalyst after used for 10.5 h.

This indicates that the carbon deposits grow from the outlet side (catalyst-rich side) to the inlet side (catalyst-poor side). Furthermore, even if the time-on-stream was extended from 6 h to 10.5 h, there was a small amount of growth of the carbon deposits, but it was not proportional to the time-on-stream. Since the appearance of carbon deposits in the inlet side (highlighted with a blue line) and in the outlet side (highlighted with a red line) of the reactor seemed to be different, each catalyst from the outlet and inlet side was characterized.

Those samples were analyzed using FE-SEM (**Figures 10 (A) – (F)**, respectively). After the reaction, the sample in the inlet side of the catalyst pretreated for 0 h showed a net-shaped wire (Figure 10 (A)), but the growth of net-shaped wire was apparent at the outlet side of the catalyst (Figure 10 (B)). This indicates that the wire seemed to grow on the outlet side of the catalyst. When the pretreatment time was set to 5 h, wire-like substances could not be detected in the inlet side of the catalyst (Figure 10 (C)). However, the growth of a wire-like substance was detected in the outlet side of the catalyst (Figure 10 (D)). When the previously used samples shown in Figure 7 were analyzed using FE-SEM, wire-like substances were evident regardless of the position of the inlet and outlet sides (Figures 7 (E) and (F). respectively). It is noteworthy that carbon deposition rather than wire-like substances was also detected. Therefore, we suggest that when a large amount of carbon deposit forms, it will cover the wire-like substance. As shown in **Figure 11**, XRD patters of the samples shown in Figures 10 (E) and (F) reveal the formation of an excess amount of carbon over metallic Ni, on both the inlet and outlet sides (Figures 11 (A) and (B), respectively), which resulted in a decreased isobutene yield, as shown in Figure 7.

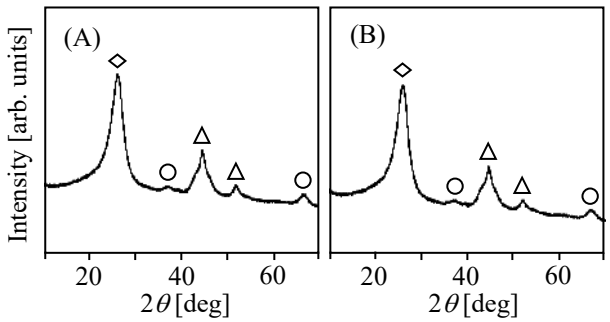


**Fig. 11** XRD patterns of NiO(20)/γ-$Al_2O_3$ previously used for obtaining the results shown in Figure 7
(A) Inlet side of the catalyst after used for 10.5 h.
(B) Outlet side of the catalyst after used for 10.5 h.
○: γ-$Al_2O_3$, △: Ni, ◇: Carbon

In order to examine these dependencies, TPO was employed. After obtaining the results shown in Figure 6, the NiO(20)/γ-$Al_2O_3$ pretreated for 0 h showed a $CO_2$-desorption amount from the outlet side of the sample (highlighted with a red line) that was evidently greater than that from the inlet side (highlighted with a blue line) (**Figure 12 (A)**). However, based on the desorption temperature, the properties of the carbon deposits from both the inlet and outlet sides of these catalysts seemed similar. In contrast, after obtaining the results shown in Figure 6, the $CO_2$-desorption amounts from both sides of NiO(20)/γ-$Al_2O_3$ pretreated for 5 h were similar (**Figure 12 (B)**). However, the desorption temperature from the inlet side of the sample (highlighted with a blue line) was lower than that from the outlet side (highlighted with a red line). Therefore, the complex formation of various carbon deposits seemed to contribute to an evident enhancement in the yield of isobutene, as shown in Figure 6.

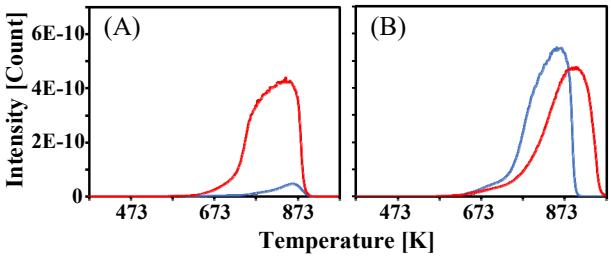


**Fig. 12** TPO images of NiO(20)/γ-$Al_2O_3$ previous used for obtaining the results shown in Figure 6
(A) The catalyst pretreated for 0 h.
(B) The catalyst pretreated for 5 h.
Blue and red lines: from inlet and outlet sides, respectively.

In the present study, we focused on the formation of carbon deposits together with the reduction from NiO to metallic Ni during the dehydrogenation of isobutane. It should be noted that the yield of isobutene was enhanced during the dehydrogenation in the absence of $CO_2$, indicating that the effect of adding $CO_2$ into the feedstream according to eq. (3) did not significantly affect the improvement of the isobutene yield in the present study. Therefore, different properties of carbon deposits formed from the interaction between isobutane and metallic Ni could have enhanced the yield of isobutene. Nickel metal in the presence of hydrocarbons is known to precipitate various carbon species such as carbon nanowires (Liao and Ting, 2004), carbon nanotubes (Zhang *et al*., 2008), carbon filament (Mok *et al*., 2013; Charisiou *et al*., 2019), and carbon films (Ji *et al*., 2019). It is generally accepted that the formation of carbon films results in a general deactivation (Ji *et al*., 2019). Carbon nanotube-like deposits that formed around Ni particles during dehydrogenation are expected to protect the Ni particles from sintering. Furthermore, it is also expected that the reactant can contact the catalyst surface relatively smoothly through the space between the nanotubes, which simultaneously results in suitable dehydrogenation that promotes the reduction of NiO to metallic Ni.

For another explanation of the present enhancement of isobutene yield, we focus on the unique properties between Ni and carbon species. Carbon nanotubes are produced by the contribution of Ni, followed by the formation of a matching Ni compound (Ni-Tip-carbon) via the tip-growth mechanism shown in **Figure 13** (Abdi, *et al*., 2006). Although this Ni-Tip-carbon is an analogue to Ni-carbide, Figure 5 (B) shows that Ni-Tip-carbon may be formed in the NiO(x)/γ-$Al_2O_3$ previously employed in the activity test. As shown in Figure 5 (B), metallic Ni was evidently detected in these catalysts. However, the main peak due to metallic Ni at around $2\theta = 44$ degrees in Figure 5(B) matched the main peak due to $Ni_3C$ (nickel carbide) (Uhlig *et al*., 2013). Furthermore, a similar carbide species is known to be an active site for the selective dehydrogenation of n-butane (Neylon *et al*., 1999; Kwon *et al*., 2000).

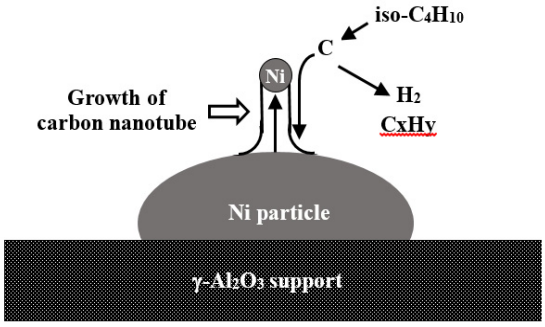


**Fig. 13** Concept illustration of tip-growth mechanism

Therefore, Ni-Tip-carbon may be one of the most plausible candidates for the active species. It was reasonable in the present study that Ni-Tip-carbon and carbon nanowires were formed during dehydrogenation. Based on the formation of these carbon species, the maximum activity at around NiO(20)/γ-$Al_2O_3$ shown in Figure 2 can be explained as follows. With the loading of as much as 20wt% NiO, the Ni-Tip-carbon grows, resulting in an enhancement of the catalytic activity. If NiO loading exceeds 20%, such as in the case of NiO(30)/γ-$Al_2O_3$, the activity decreases since the inactive carbon nanotubes or simple carbon deposition cover the active Ni-Tip-carbon. Thus, the catalytic activity using NiO(5)/γ-$Al_2O_3$ was lower than that using NiO(20)/γ-$Al_2O_3$ due to the insufficient formation of the active Ni-Tip-carbon. It is noteworthy that the catalytic activity using NiO(30)/γ-$Al_2O_3$ was evidently lower when using NiO(5)/γ-$Al_2O_3$. This is because when using NiO(5)/γ-$Al_2O_3$, the formation of the active Ni-Tip-carbon takes precedence over the formation of the inactive carbon nanotube, resulting in an enhancement of the catalytic activity. Conversely, when NiO(30)/γ-$Al_2O_3$ is used, the formation of the inactive carbon nanoparticles exceeds the formation of the Ni-Tip-carbon, resulting in a decrease in the catalytic activity. Based on these results, it is understandable that both NiO(5)/γ-$Al_2O_3$ and NiO(30)/γ-$Al_2O_3$ exhibited lower activity, as shown in Figure 2. In using NiO(20)/γ-$Al_2O_3$, a suitable formation balance of both the inactive carbon nanotube and the active Ni-Tip-carbon resulted in maximum activity, as shown in Figure 2. Furthermore, the decrease in the isobutene yield at 10.5 h on-stream shown in Figure 7 can be explained by an excess formation of the inactive carbon nanotube, which covered the active Ni-Tip-carbon.

Finally, in order to examine the regeneration behavior of NiO(20)/γ-$Al_2O_3$, the normal activity test as shown in Figure 2 was performed using this catalyst, and then the catalyst was regenerated at 823 K for 1 h under an oxygen flow at 12.5 mL/h, followed by the usual reaction shown in Figure 2. As shown in **Figure 14**, the regeneration using the $O_2$ in NiO(20)/γ-$Al_2O_3$ resulted in no further enhancement of iso-$C_4H_8$ yield while rather stable activity was observed following 6 h on-stream. Therefore, in order to selectively eliminate the inactive carbon nanowire, the regeneration conditions should be carefully considered.

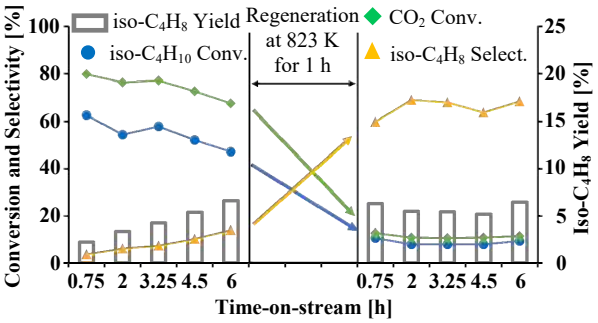


**Fig. 14** Regeneration behavior of NiO(20)/γ-$Al_2O_3$ previously used under the conditions shown in Figure 2

## Conclusions

When the direct dehydrogenation of isobutane was performed in both the presence and absence of carbon dioxide on a NiO/**γ**-$Al_2O_3$ catalyst, the yield of isobutene was significantly improved as the carbon deposition progressed, which is unlike other usual catalytic reactions. The following two points were suggested as the causes of the activity improvement. First, it was proposed that the carbon nanotubes formed during the present dehydrogenation could suppress the sintering of metallic Ni and improve the catalytic activity. Furthermore, the second cause was proposed to improve the catalytic activity because Ni carbide species possessing high activity for dehydrogenation were formed during the present dehydrogenation. Further study on the present unique enhancement of the catalytic activity is now in progress.

## Acknowledgement

This study was supported by JSPS KAKENHI Grant Number JP20K056221 and by the Research Clusters Program of Tokushima University (1702001), for which we are grateful.

**Literature Cited**

Abdi, Y., J. Koohsorkhi, J. Derakhshandeh, S. Mohajerzadeh, H. Hoseinzadegan, M. D. Robertson, J. C. Bennett, X. Wu and H. Radamson; "PECVD-grown Carbon Nanotubes on Silicon Substances with a Nickel-seeded Tip-growth structure," *Mater. Sci. Eng. C*, **26**, 1219-1223 (2006)

Carrà, S. and L. Forni; "Catalytic Dehydrogenation of C4 Hydrocarbons over Chromia-Alumina," *Catal. Rev*., **5**, 159-198 (1971)

Charisiou, N. D., V. Sebastian, S. J. Hinder, M. A. Baker, K. Polychronopoulou and M. A. Goula; "Ni Catalysts Based on Attapulgite for Hydrogen Production through the Glycerol Steam Reforming Reaction," *Catalysts*, **9**, 650-669 (2019)

Ding, J., R. Shao, J. Wu, Z. Qin and J. Wang; "Coupling Dehydrogenation of Isobutane to Produce Isobutene in Carbon Dioxide over NiO/γ-$Al_2O_3$ Catalyst," *React. Kinet. Mech. Catal*., **101**, 173-181 (2010)

Ehiro, T., A. Itagaki, H. Misu, M. Kurashina, K. Nakagawa, M. Katoh, Y. Katou, W. Ninomiya and S. Sugiyama; "Oxidative Dehydrogenation of Isobutane to Isobutene on Metal-Doped MCM-41 Catalysts," *J. Chem. Eng. Japan*, **49**, 136-143 (2016a)

Grzybowska, B., J. Słoczyński, R. Grabowski, K. Wcislo, A. Kozłowska, J. Stoch and J. Zieliński; "Chromium Oxide/Alumina Catalysts in Oxidative Dehydrogenation of Isobutane," *J. Catal*., **178**, 687-700 (1998)

Ji, K., F. Meng, J. Xun, P. Liu, K. Zhang, Z. Li and J. Gao; "Carbon Deposition Behavior of Ni Catalyst Prepared by Combustion Method in Slurry Methanation Reaction," *Catalysts*, **9**, 570-581 (2019)

Jibril, B. Y., N. O. Elbashir, S. Al-Zahrani and A. E. Abasaeed; "Oxidative Dehydrogenation of Isobutane on Chromium Oxide-Based Catalyst," *Chemical Engineering and Processing*, **44**, 835-840 (2005)

Kato, Y., H. Misu, S. Shimazu, M. Katoh, W. Ninomiya and S. Sugiyama; "Introduction of a Small Amount of Chromium to Enhance the Catalytic Performance of SBA-15 for the Oxidative Dehydrogenation of Isobutane to Isobutene," *J. Chem. Eng. Japan*, **51**, 400-406 (2018)

Kato, Y., S. Nitta, S. Shimazu, M. Kurashina, M. Katoh, W. Ninomiya and S. Sugiyama; "Effect of Introduction of Trace Amount of Chromium Species in Improving Catalytic Performance of MCM-48 in Oxidative Dehydrogenation of Isobutane," *J. Chem. Eng. Japan*, **52**, 99-105 (2019a)

Kato, Y., S. Nitta, K. Oribe, M. Katoh, W. Ninomiya and S. Sugiyama; "Modifying SBA-15 with Binary Elements of Chromium and Molybdenum for Improved Catalytic Performance in the Oxidative Dehydrogenation of Isobutane to Isobutene," *J. Chem. Eng. Japan*, **52**, 521-527 (2019b)

Korhonen, S. T., S. M. K. Airaksinen, M. A. Bañares and A. O. I. Krause; "Isobutane Dehydrogenation on Zirnonia-, Alumina- and Zironia/Alumina-Supported Chomia Catalysts," *Appl. Catal. A; Gen.*, **333**, 30-41 (2007)

Kwon, H., L. T. Thompson, J. Eng, Jr. and J. G. Chen; "n-Butane Dehydrogenation over Vanadium Carbides: Correlating catalytic and Electronic Properties," *J. Catal*., **190**, 60-68 (2000)

Liao, K. and J. Ting; "Effects of Ni-catalyst Characteristics on the Growth of Carbon Nanowires," *Carbon*, **42**, 509-514 (2004)

Mok, Y. S., E. Jwa and Y. J. Hyun; "Regeneration of $C_4H_{10}$ Dry Reforming Catalyst by Nonthermal Plasma," *J. Energy Chem*., **22**, 394-402 (2013)

Nagai, K.; "New Development in the Production of Methyl Methacrylate," *Appl. Catal. A; Gen.*, **221**, 367-377 (2001)

Neylon, M. K., S. Choi, H. Kwon, K. E. Kurry and L. T. Thompson; "Catalytic Properties of Early Trensition Metal Nitrides and Carbides: n-Butane Hydrogenolysis, Dehydrogenation and Isomerization," *Appl. Catal. A; Gen,* **183**, 253-263 (1999)

Ninomiya, W.; "Industrialised Polyoxometalate Catalyst-Heteropolyacid Catalyst for Selective Oxidation of Methacrolein to Methacrylic Acid," *Catal. (Shokubai)*, **56**, 360-366 (2014)

Ohtani, B.; "Standard Research Method for Photo Catalyst," p. 289, Tokyo Tosho Co., Ltd., Japan (2005)

Okada, Y.; "Study on Catalytic Reaction Using Porous Oxide with Uniform Pore Distribution," *Doctoral Thesis, Yokohama National University*, 2-10 (2005)

Sugiyama, S., Y. Nitta, Y. Furukawa, A. Itagaki, T. Ehiro, K. Nakagawa, M. Katoh, Y. Katou, S. Akihara and W. Ninomiya; "Oxidative Dehydrogenation of Isobutane to Isobutene on FSM-16 Doped with Cr and Related Catalysts," *J. Chem. Chem. Eng.*, **7**, 1014-1020 (2013)

Uhlig, S., R. Struis, H. Schmid-Engel, J. Bock, A.-C. Probst, O. Freitag-Weber, I. Zizak, R. Chernikov and G. Schultes; "Piezoresistive Ni:a-C:H Thin Films Containing hcp-Ni or $Ni_3C$ Investigated by XRD, EXAFS, and Wavelet Analysis," *Diam. Relat. Mater.*, **34**, 25-35 (2013)

Zhang, Q., Y. Liu, L. Hu, W. Qian, G. Luo and F. Wei; "Synthesis of Thin-walled Carbon nanotubes from Methane by Changing the Ni/Mo Ratio in a Ni/Mo/MgO Catalyst," *New Carbon Mater*., **23**, 319-325 (2008)